Plasmonic trapping and tuning of a gold nanoparticle dimer

Shen, Z; SU, L

Plasmonic trapping and tuning of a gold nanoparticle dimer

Zhe Shen[1] and Lei Su[1, 2*]

[1]*Department of Electrical Engineering & Electronics, University of Liverpool, Liverpool L69 3GJ, United Kingdom*
[2]*School of Engineering and Materials Science, Queen Mary University of London, London E1 4NS, United Kingdom*
*l.su@qmul.ac.uk

Abstract: We demonstrate theoretically the trapping and manipulating of a gold nanoparticle dimer, using surface plasmon excited by a focused linearly-polarized laser beam on a silver film. We use both finite-difference time-domain force analysis and Maxwell stress tensor to show that the gold nanoparticle dimer can be trapped by a virtual probe pair. A formula is derived to represent the plasmonic field, suggesting that the gap between the two gold nanoparticles in the dimer can be controlled, for example, by tuning the excitation-laser wavelength. We further test our theory by successfully trapping nanoparticle dimers formed by nanospheres and nanorods. The controllable gap in between the nanoparticles can lead to tunable localized surface plasmon resonances, and this may find new exciting applications in plasmonic sensing or in lab-on-a-chip devices.

References and links

1. I. Romero, J. Aizpurua, G. W. Bryant, and F. J. G. de Abajo, "Plasmons in nearly touching metallic nanoparticles: singular response in the limit of touching dimers," Opt. Express **14**, 9988-9999 (2006).
2. J. I. Chen, Y. Chen, and D. S. Ginger, "Plasmonic nanoparticle dimers for optical sensing of DNA in complex media," J. Am. Chem. Soc. **132**, 9600-9601 (2010).
3. T. Atay, J. H. Song, and A. V. Nurmikko, "Strongly interacting plasmon nanoparticle pairs: From dipole-dipole interaction to conductively coupled regime," Nano Lett. **4**, 1627-1631 (2004).
4. P. Nordlander, C. Oubre, E. Prodan, K. Li, and M. I. Stockman, "Plasmon hybridization in nanoparticle dimers," Nano Lett. **4**, 899-903 (2004).
5. C. E. Talley, J. B. Jackson, C. Oubre, N. K. Grady, C. W. Hollars, S. M. Lane, T. R. Huser, P. Nordlander, and N. J. Halas, "Surface-enhanced Raman scattering from individual Au nanoparticles and nanoparticle dimer substrates," Nano Lett. **5**, 1569-1574 (2005).
6. W. Li, P. H. Camargo, X. Lu, and Y. Xia, "Dimers of silver nanospheres: facile synthesis and their use as hot spots for surface-enhanced Raman scattering," Nano Lett. **9**, 485-490 (2009).
7. A. Kinkhabwala, Z. F. Yu, S. H. Fan, Y. Avlasevich, K. Mullen, and W. E. Moerner, "Large single-molecule fluorescence enhancements produced by a bowtie nanoantenna," Nat. Photonics **3**, 654-657 (2009).
8. B. Pettinger, B. Ren, G. Picardi, R. Schuster, and G. Ertl, "Nanoscale probing of adsorbed species by tip-enhanced Raman spectroscopy," Phys. Rev. Lett. **92,** 096101 (2004).
9. J. M. McMahon, A. I. Henry, K. L. Wustholz, M. J. Natan, R. G. Freeman, R. P. Van Duyne, and G. C. Schatz, "Gold nanoparticle dimer plasmonics: finite element method calculations of the electromagnetic enhancement to surface-enhanced Raman spectroscopy," Anal. Bioanal. Chem. **394**, 1819-1825 (2009).
10. D. C. Marinica, A. K. Kazansky, P. Nordlander, J. Aizpurua, and A. G. Borisov, "Quantum plasmonics: nonlinear effects in the field enhancement of a plasmonic nanoparticle dimer," Nano Lett. **12**, 1333-1339 (2012).
11. V. V. Thacker, L. O. Herrmann, D. O. Sigle, T. Zhang, T. Liedl, J. J. Baumberg, and U. F. Keyser, "DNA origami based assembly of gold nanoparticle dimers for surface-enhanced Raman scattering," Nat. Commun. **5**, 3448 (2014).
12. R. W. Taylor, T. C. Lee, O. A. Scherman, R. Esteban, J. Aizpurua, F. M. Huang, J. J. Baumberg, and S. Mahajan, "Precise subnanometer plasmonic junctions for SERS within gold nanoparticle assemblies using cucurbit[n]uril "glue"," ACS nano **5**, 3878-3887 (2011).
13. J. Mertens, A. L. Eiden, D. O. Sigle, F. M. Huang, A. Lombardo, Z. P. Sun, R. S. Sundaram, A. Colli, C. Tserkezis, J. Aizpurua, S. Milana, A. C. Ferrari, and J. J. Baumberg, "Controlling subnanometer gaps in plasmonic dimers using graphene," Nano Lett. **13**, 5033-5038 (2013).
14. A. Ashkin, J. M. Dziedzic, J. E. Bjorkholm, and S. Chu, "Observation of a single-beam gradient force optical trap for dielectric particles," Opt. Lett. **11**, 288-290 (1986).
15. D. G. Grier, "A revolution in optical manipulation," Nature **424**, 810-816 (2003).

16. Q. W. Zhan, "Trapping metallic Rayleigh particles with radial polarization," Opt. Express **12**, 3377-3382 (2004).
17. K. Svoboda, and S. M. Block, "Optical trapping of metallic Rayleigh particles," Opt. Lett. **19**, 930-932 (1994).
18. L. Huang, H. L. Guo, J. F. Li, L. Ling, B. H. Feng, and Z. Y. Li, "Optical trapping of gold nanoparticles by cylindrical vector beam," Opt. Lett. **37**, 1694-1696 (2012).
19. G. Volpe, R. Quidant, G. Badenes, and D. Petrov, "Surface plasmon radiation forces," Phys. Rev. Lett. **96**, 238101 (2006).
20. M. Righini, A. S. Zelenina, C. Girard, and R. Quidant, "Parallel and selective trapping in a patterned plasmonic landscape," Nat. Phys. **3**, 477-480 (2007).
21. R. Quidant, and C. Girard, "Surface-plasmon-based optical manipulation," Laser Photonics Rev. **2**, 47-57 (2008).
22. K. Wang, E. Schonbrun, and K. B. Crozier, "Propulsion of gold nanoparticles with surface plasmon polaritons: evidence of enhanced optical force from near-field coupling between gold particle and gold film," Nano Lett. **9**, 2623-2629 (2009).
23. W. Zhang, L. Huang, C. Santschi, and O. J. F. Martin, "Trapping and sensing 10 nm metal nanoparticles using plasmonic dipole antennas," Nano Lett. **10**, 1006-1011 (2010).
24. M. L. Juan, M. Righini, and R. Quidant, "Plasmon nano-optical tweezers," Nat. Photonics **5**, 349-356 (2011).
25. B. J. Roxworthy, K. D. Ko, A. Kumar, K. H. Fung, E. K. C. Chow, G. L. Liu, N. X. Fang, and K. C. Toussaint, "Application of plasmonic bowtie nanoantenna arrays for optical trapping, stacking, and sorting," Nano Lett. **12**, 796-801 (2012).
26. P. T. Lin, H. Y. Chu, T. W. Lu, and P. T. Lee, "Trapping particles using waveguide-coupled gold bowtie plasmonic tweezers," Lab on a chip **14**, 4647-4652 (2014).
27. Y. Q. Zhang, J. Wang, J. F. Shen, Z. S. Man, W. Shi, C. J. Min, G. H. Yuan, S. W. Zhu, H. P. Urbach, and X. C. Yuan, "Plasmonic hybridization induced trapping and manipulation of a single Au nanowire on a metallic surface," Nano Lett. **14**, 6430-6436 (2014).
28. C. Min, Z. Shen, J. Shen, Y. Zhang, H. Fang, G. Yuan, L. Du, S. Zhu, T. Lei, and X. Yuan, "Focused plasmonic trapping of metallic particles," Nat. Commun. **4**, 2891 (2013).
29. S. A. Maier, M. L. Brongersma, P. G. Kik, S. Meltzer, A. A. G. Requicha, and H. A. Atwater, "Plasmonics - a route to nanoscale optical devices," Advanced materials **13**, 1501-1505 (2001).
30. H. Raether, *Surface Plasmons on Smooth and Rough Surfaces and on Gratings* (Springer, 1988).
31. A. Bouhelier, F. Ignatovich, A. Bruyant, C. Huang, G. C. D. Francs, J. C. Weeber, A. Dereux, G. P. Wiederrecht, and L. Novotny, "Surface plasmon interference excited by tightly focused laser beams," Opt. Lett. **32**, 2535-2537 (2007).
32. F. D. Stefani, K. Vasilev, N. Bocchio, N. Stoyanova, and M. Kreiter, "Surface-plasmon-mediated single-molecule fluorescence through a thin metallic film," Phys. Rev. Lett. **94**, 023005 (2005).
33. P. B. Johnson, and R. W. Christy, "Optical Constants of Noble Metals," Phys. Rev. B. **6**, 4370-4379 (1972).
34. L. Novotny, and B. Hecht, *Principles of Nano-optics* (Cambridge University Press, 2012).
35. B. Richards, and E. Wolf, "Electromagnetic diffraction in optical systems .2. Structure of the image field in an aplanatic system," Proc. R. Soc. A. **253**, 358-379 (1959).
36. E. Wolf, "Electromagnetic diffraction in optical systems .1. An integral representation of the image field," Proc. R. Soc. A. **253**, 349-357 (1959).
37. Q. W. Zhan, "Evanescent Bessel beam generation via surface plasmon resonance excitation by a radially polarized beam," Opt. Lett. **31**, 1726-1728 (2006).
38. A. D. Rakic, A. B. Djurisic, J. M. Elazar, and M. L. Majewski, "Optical properties of metallic films for vertical-cavity optoelectronic devices," Applied optics **37**, 5271-5283 (1998).
39. E. C. Le Ru, and P. G. Etchegoin, "Rigorous justification of the [E](4) enhancement factor in surface enhanced Raman spectroscopy," Chem. Phys. Lett. **423**, 63-66 (2006).

1. Introduction

Gold nanoparticle dimers have attracted much attention in plasmonic sensing, because strong localized surface plasmon resonance (LSPR), also known as hot spots, can be excited in the nanoscale gap between the two gold nanoparticles [1-4]. This makes them useful for field enhancement in sensing and measurement applications, such as surface enhanced Raman spectroscopy (SERS) [5,6]. Compared to other nanostructures for hot-spot excitation, including nano-antennae [7] and metallic nano-tips [8], gold nanoparticles offer great flexibility and can be used for intracellular detections. In SERS, the nanoscale gap or void formed by gold nanostructures is important for field enhancement [5]. In general, the field enhancement factor is inversely-proportional to the size of the gap [9,10]. There are several methods that can achieve desirable nanoparticle dimers for LSPR generation, for example, using self-assembly of gold nanoparticles. However, the gap distance is pre-determined and is

unable to be changed afterwards. In terms of controlling the size of the nano-gap in a dimer, nanomaterials such as DNA [11], cucurbit[n]uril [12] and graphene [13] were proposed as binding materials. However, these may limit the applications and can become a source of noise during measurements. Therefore, in this study, we aim to find an alternative way for a controllable nanoparticle gap for LSPR excitation.

Optical trapping, or optical tweezers, has been applied in manipulating transparent objects ranging in size from tens of nanometers to tens of micrometers, by utilizing the gradient forces generated from focused laser beams [14]. Optical-tweezer arrays are capable of trapping and moving multiple particles [15]. However, it is very challenging to manipulate metallic particles using traditional optical trapping methods due to the high scattering from them. Although beam shaping method was used to trap metallic Rayleigh particles, i.e. particles with a radius less than the incident wavelength [16-18], the tuning of the nanoscale gap is very difficult, as is constrained by the diffraction limit of the light.

Recently, plasmonic trapping was used to manipulate metallic particles ranging in size from tens of nanometers to hundreds of micrometers [19-29]. In these studies, the trapping force was enhanced to move gold particles, based on the coupling of surface plasmon polaritions (SPP) and localized surface plasmon (LSP). In our previous work, focused plasmonic trapping of metallic particles was demonstrated by using a virtual probe on a flat gold film [28]. We showed that the enhanced LSP field was able to trap metallic particles as a result of the rapidly varying electrical field.

In this paper, we present the first study on plasmonic trapping and tuning of a gold nanoparticle dimer. We focus a linearly-polarized beam onto a silver film to excite surface plasmons (SPs). The interference between the excited SP waves forms two symmetrical virtual probes, which are used to trap two nanoparticles. To interpret the trapping process, Richard-Wolf diffraction theory and angular spectrum representation are used to calculate the plasmonic field. A relation between the virtual-probe spacing and the excitation wavelength is obtained. Subsequently, three-dimensional (3D) finite-difference time-domain (FDTD) simulations are carried out, to analyze the electrical field interacting with the gold nanoparticles. The forces are calculated using Maxwell stress tensor (MST). Both gold nanospheres and nanorods are used in our simulations to test the plamonic trapping system.

2. Theory

2.1 Plasmonic field calculation

SPs are solutions of Maxwell's equations for metal-dielectric interfaces [30]. The dispersion equation for SP, i.e. the relation between the frequency and the wave vector, is given as:

$$k_{sp} = \frac{2\pi}{\lambda_0}\sqrt{\frac{\varepsilon_2\varepsilon_m}{\varepsilon_2+\varepsilon_m}} \tag{1}$$

where λ_0 is the incident light wavelength, ε_2 and ε_m are the dielectric constants of the sample and the metal respectively.

Surface plasmon resonance (SPR) is excited when the horizontal component of the evanescent wave vector matches that of the SP:

$$k_r = \frac{2\pi}{\lambda_0}\sqrt{\varepsilon_1}\sin\theta_{sp} = k_{sp} \tag{2}$$

where θ_{sp} is the resonance angle, and ε_1 is the dielectric constant of the substrate.

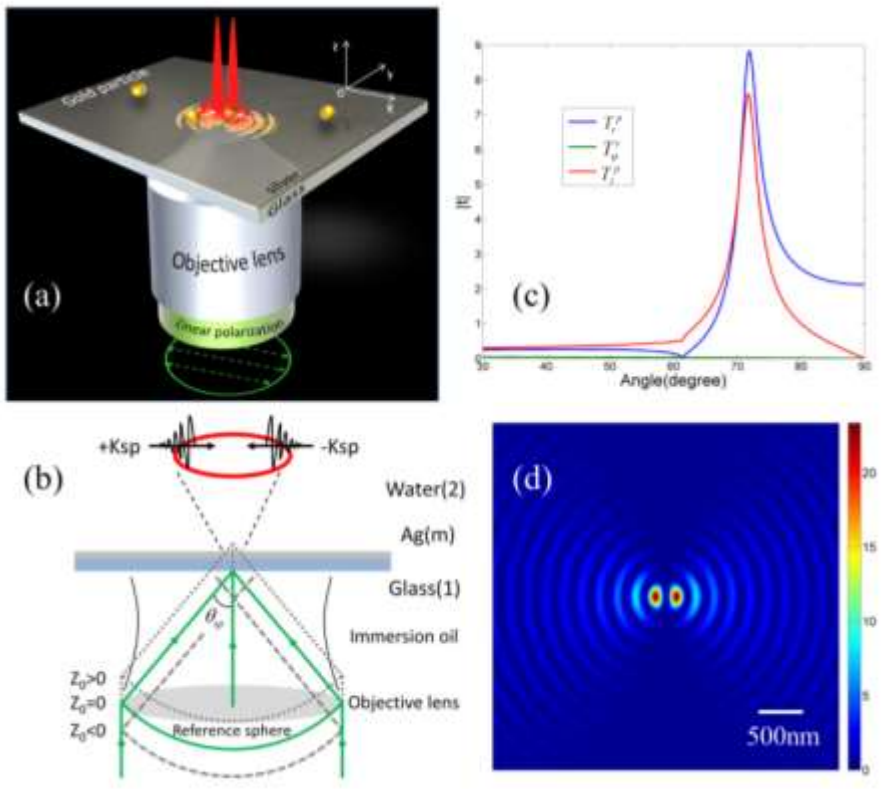

Fig. 1. (a) The proposed plasmonic trapping system. The incident light is linearly-polarized and is focused to a 45nm-thick silver film through a 1.49- NA objective lens. Green-colored arrows indicate the polarization direction of the incident light (x direction). Red-colored field is the calculated surface plasmonic field, excited by the focused linearly-polarized beam. (b) Front view of the system in x-z plane, showing the plasmonic virtual-probe pair generated by interference. 2, m and 1 indicate different substrates, and are used as subscripts in following derivations and equations. The solid green lines indicate the incident light at an angle close to θ_{sp} . Z_0 represents the distance from the laser focus to the metal film. (c) Calculated transmission coefficients as a function of incident angles for s- and p-polarization for different electrical field components. $\varepsilon_2 = 1.33$, $\varepsilon_1 = 1.515^2$, the thickness of sliver film $d = 45nm$, the dielectric constant of Ag film is -11.76+0.37i at 532nm, and the water layer thickness is 3μm. (d) Top-view of the plasmonic field (showing the electrical-field distribution 10nm above the silver layer. z_0=1μm and $f_0 = 1$ [f_0 is the filling factor and the identifier defined in Eq. (10)]

Our proposed plasmonic trapping system is shown in Fig. 1(a). The plasmonic field is excited on the Ag film by a focused linearly-polarized beam, and two virtual probes are formed for gold-nanoparticle trapping. Since the SP excitation is polarization selective (p-polarization), it has the maximum efficiency along the polarization (x direction). A simplified system (x-z plane) is shown in Fig. 1(b), where two sets of symmetrical plane waves incident at angles $\pm\theta_{sp}$ and excite a pair of counter-propagating SP waves with wave vectors $\pm k_{sp}$. The π phase delay between these two SP waves leads to a destructive interference and two enhanced lobes in the standing wave are formed [Fig. 1(b)]. Evidence of such counter-propagating waves were presented experimentally in [31,32] .

According to Fresnel functions, for Kretschmann configuration (three-layer structure: substrate-Ag-water), the transmission coefficients for E_r , E_φ and E_z transmitting through a metal film are given as [30]:

$$\begin{cases} T_r^p(\theta) = \dfrac{\varepsilon_1 k_{z2}}{\varepsilon_2 k_{z1}} \cdot \dfrac{(1+r_{m2}^p)(1+r_{1m}^p)\exp(ik_{zm}d)}{1+r_{m2}^p r_{1m}^p \exp(2ik_{zm}d)} \\ T_\varphi^s(\theta) = \dfrac{(1+r_{m2}^s)(1+r_{1m}^s)\exp(ik_{zm}d)}{1+r_{m2}^s r_{1m}^s \exp(2ik_{zm}d)} \\ T_z^p(\theta) = \dfrac{\varepsilon_1}{\varepsilon_2} \cdot \dfrac{(1+r_{m2}^p)(1+r_{1m}^p)\exp(ik_{zm}d)}{1+r_{m2}^p r_{1m}^p \exp(2ik_{zm}d)} \end{cases} \quad (3)$$

where $k_{zi} = k_0\sqrt{\varepsilon_i - \varepsilon_1 \cdot \sin^2\theta}$ is the longitudinal wave vector, ε_1 is the dielectric constant of the substrate, d is the thickness of the metal film, r_{ij}^s and r_{ij}^p are the Fresnel reflection coefficients for s-polarization and p-polarization at the i (incident) and j interfaces respectively.

Figure 1(c) shows that the transmission coefficients as a function of the light incident angles for different electrical fields at both s- and p-polarizations. The dielectric constant of Ag is obtained according to Johnson and Christy [33]. It can be seen that T_φ is relatively small over the entire angle range. This suggests that E_φ is significantly attenuated by the Ag film. Compared to T_φ, both T_r and T_z are relatively large with the values of 7.6 and 8.9 at $\theta_{sp} = 72.3^\circ$. The maximum incident angle can be achieved by 1.49- NA objective lens is 79.6°, which is sufficient for SPP excitation.

In a strongly focused system as shown in Fig. 1(a), the angular spectrum representation shows how the field propagates and how it is mapped onto other planes [34]:

$$E_t(x,y,z) = \int_{k_x}\int_{k_y} E\left(k_x,k_y\right)\exp\left[i\left(k_x x + k_y y \pm k_z z\right)\right]dk_x dk_y \quad (4)$$

Where k_x, k_y and k_z are the transverse and longitudinal components of the wave vector respectively, and $E\left(k_x,k_y\right)$ is the incident electromagnetic field. Considering asymptotic far-zone approximation of this field, Eq. (4) becomes

$$E_t(x,y,z) = \frac{ife^{-ik_1 f}}{2\pi}\iint_{k_x,k_y} E_t^\infty(k_x,k_y)\frac{1}{k_{z2}}e^{i\left(k_x x + k_y y + k_z z\right)}dk_x dk_y \quad (5)$$

Invoking the boundary conditions at $Z = Z_0$ in Eq. (5), and using Fresnel coefficients, we obtain,

$$E_t^\infty = E_{inc}(k_x,k_y)e^{i(k_{z1}-k_{z2})z_0}\begin{bmatrix} t^s {k_y}^2 + t^p {k_x}^2 k_{z2}/k_2 \\ -t^s k_x k_y + t^p k_x k_y k_{z2}/k_2 \\ 0 - t^p({k_x}^2 + {k_y}^2)k_x/k_2 \end{bmatrix}\frac{k_{z2}}{k_{z1}}\frac{\sqrt{k_{z1}/k_1}}{{k_x}^2 + {k_y}^2} \quad (6)$$

where t^p and t^s are the transmission coefficients of the p-polarization and s-polarization light respectively. We are interested in the longitudinal component in Eq (6),

$$E_z^\infty = -E_{inc}(k_x,k_y)e^{i(k_{z1}-k_{z2})z_0}t^p\frac{k_x}{k_2}\frac{k_{z2}}{k_{z1}}\sqrt{k_{z1}/k_1} \quad (7)$$

In the following analysis, we follow the theory established by Richards and Wolf and use cylindrical coordinates [35,36]:

$$E_t(\rho,\varphi,z)=\frac{ife^{-ik_1 f}}{2\pi}\int_0^{\theta_{\max}}\int_0^{2\pi}-E_{inc}(\theta,\phi)e^{i(k_{z1}-k_{z2})z_0}t^p e^{ik_2\rho\sin\theta\cos(\phi-\varphi)}e^{izk_{z2}}\frac{k_2^{\,2}}{k_1}\sin^2\theta\sqrt{\cos\theta}\cos\phi d\theta d\varphi \tag{8}$$

By using the mathematical identity

$$\int_0^{2\pi}\cos\phi\exp[ik_2\rho\sin\theta\cos(\phi-\varphi)]=2\pi i\cos\varphi J_1(k_2\rho\sin\theta) \tag{9}$$

where $J_1(x)$ is the first order Bessel function of the first kind, we have

$$E_t(\rho,\varphi,z)=\cos\varphi fe^{-ik_1 f}\int_0^{\theta_{\max}}E_{inc}(\theta,\phi)e^{i(k_{z1}-k_{z2})z_0}t^p J_1(k_2\rho\sin\theta)e^{ik_{z2}z}\frac{k_2^{\,2}}{k_1}\sin^2\theta\sqrt{\cos\theta}d\theta d\varphi \tag{10}$$

Assuming the incident light as a linearly-polarized Gaussian beam, we can obtain

$$E_{inc}(\theta,\phi)=E_0e^{-f^2\sin^2\theta/\omega_0^{\,2}}=E_0e^{-\sin^2\theta/f_0^{\,2}\sin^2\theta_{\max}}=E_0e^{-\frac{n_1^{\,2}\sin^2\theta}{(f_0NA)^2}} \tag{11}$$

where $f_0=\dfrac{w_0}{f\sin\theta_{\max}}$ is the filling factor and the identifier [34], and n_1 is the refractive index of the substrate. The plasmonic electrical field in Eq. (10) becomes

$$E_t(\rho,\varphi,z)=\cos\varphi fe^{-ik_1 f}\int_0^{\theta_{\max}}E_0e^{-\frac{n_1^{\,2}\sin^2\theta}{(f_0NA)^2}}e^{i(k_{z1}-k_{z2})z_0}t^p J_1(k_2\rho\sin\theta)e^{ik_{z2}z}\frac{k_2^{\,2}}{k_1}\sin^2\theta\sqrt{\cos\theta}d\theta \tag{12}$$

where ρ is the distance from the excitation point, φ is the angle with respect to the polarization direction and z is the distance to the metal film, k_1 and k_2 are the propagating wave vectors in the substrate and in the sample respectively, subscript z indicates the longitudinal component, and t^p is the transmission coefficient defined in Eq. (3). Given z=0.01μm, z_0=1μm, the calculated plasmonic field is shown in Fig. 1(d). The fringe period shown in Fig. 1(d) is approximately 185nm, which is in close agreement with the half SP wavelength.

2.2 Total electromagnetic force calculation for particles in the plasmonic field

The electromagnetic force on particles is the Lorentz force:

$$\vec{f}=\rho\vec{E}+\vec{J}\times\vec{B} \tag{13}$$

Based on Maxwell equations, Eq. (12) can be written as

$$\vec{f}=\varepsilon[(\nabla\cdot\vec{E})\vec{E}-\vec{E}\times(\nabla\times\vec{E})]+\frac{1}{\mu}[(\nabla\cdot\vec{B})\vec{B}-\vec{B}\times(\nabla\times\vec{B})]-\varepsilon\frac{\partial(\vec{E}\times\vec{B})}{\partial t} \tag{14}$$

Using vector calculus identity $\frac{1}{2}\nabla(\vec{A}\cdot\vec{A})=\vec{A}\times(\nabla\times\vec{A})+(\vec{A}\cdot\nabla)\vec{A}$, we have

$$\vec{f}=\nabla[\varepsilon(\vec{E}\vec{E})-\frac{\varepsilon}{2}\vec{I}E^2+\frac{1}{\mu}(\vec{B}\vec{B})-\frac{1}{2\mu}\vec{I}B^2]-\varepsilon\frac{\partial(\vec{E}\times\vec{B})}{\partial t} \tag{15}$$

where $\vec{I}$ is a unit tensor.

Using Poynting Vector $\vec{S}=\vec{E}\times\vec{H}=\frac{1}{\mu}\vec{E}\times\vec{B}$ in Eq. (15), we can obtain

$$\vec{f}=\nabla\cdot\vec{T}-\varepsilon\frac{\partial(\vec{E}\times\vec{B})}{\partial t}=\nabla\cdot\vec{T}-\varepsilon\mu\frac{\partial\vec{S}}{\partial t} \tag{16}$$

Where $\vec{T} = \varepsilon\vec{E}\vec{E} + \mu\vec{H}\vec{H} - \frac{\vec{I}}{2}(\varepsilon\left|\vec{E}\right|^2 + \mu\left|\vec{H}\right|^2)$ represents the MST matrix. In scalar form, the MST matrix is written as $\sigma_{ij} = \frac{1}{4\pi}[E_i E_j + H_i H_j - \frac{1}{2}(E^2 + H^2)\delta_{ij}]$, where δ_{ij} is Kronecker delta, and $\vec{n}$ is a unit vector normal to ds, which is the small area on particle surface.

The total electromagnetic force (Lorentz force) on the particle, given in Eq. (10), can be described as

$$\vec{F} = \int_v \vec{f}\,dv = \int_v \nabla\cdot\vec{T}\,dv - \varepsilon\mu\int_v \frac{\partial\vec{S}}{\partial t}dv \tag{17}$$

According to the divergence theorem $\int_v \nabla\cdot\vec{A}dv = \oint_s \vec{A}\cdot\vec{n}ds$, Eq. (17) becomes

$$\vec{F} = \oint_s \vec{T}\cdot\vec{n}ds - \varepsilon\mu\frac{\partial}{\partial t}\int_v \vec{S}dv \tag{18}$$

In a static electromagnetic field, $\frac{\partial\vec{S}}{\partial t} = 0$ (average over time), and then the total average force is

$$\left\langle\vec{F}\right\rangle = \left\langle\oint_s \vec{T}\cdot\vec{n}ds\right\rangle \tag{19}$$

According to the electrical field distribution obtained in our FDTD simulation, the MST formula can be used to calculate the electromagnetic forces exerted on the gold nanoparticle, as both the electrical and magnetic field can be obtained directly from the simulation data.

3. Results and discussion

We firstly calculated the average force using Eq. (19). 5nm grids were used in the FDTD simulation and the electromagnetic fields in the 3D space can be obtained. The total force was the combination of the individual force calculated for each surface point on the nanoparticle. Fig. 2 showed the calculated force in x-z plane. Since the field distribution was symmetrical with respect to x-z plane, forces in y direction cancelled each other. Therefore, the force distribution in Fig. 2 indicated the actual force exerted on the particles. In Fig. 2(a), when a single particle was considered and placed on the left virtual probe (0.1μm off the center), the force direction was in negative z direction. This suggested that the particle can be stably trapped by the virtual probe on the left. In Fig. 2(b), a gold nanosphere was placed slightly off the center and to the left of the virtual probe. Apart from the main force in the negative Z direction, there was additionally forces exerted on the particle in positive x direction (white arrow), which moved the particle to the left virtual probe. Then we examined the situation when the second particle was introduced into the system as was shown in Fig. 2(c). We found that these two particles were trapped by pulling forces to the surface due to enhanced localized field of the virtual probes. This proved that the virtual probe pair in our model formed two trapping wells for gold nanoparticles. This further suggested that the spacing between the two particles can be adjusted by changing the lobe locations in the plasmonic field. In our simulation, the virtual probe spacing was approximately 210nm and the radius of the nanosphere was 100nm. These resulted in a 10nm gap [Fig.2 (c)]. In practice, the particle size and shape could be irregular. Nevertheless, our simulations suggested that the spacing tuning of a dimer was possible in plasmonic trapping.

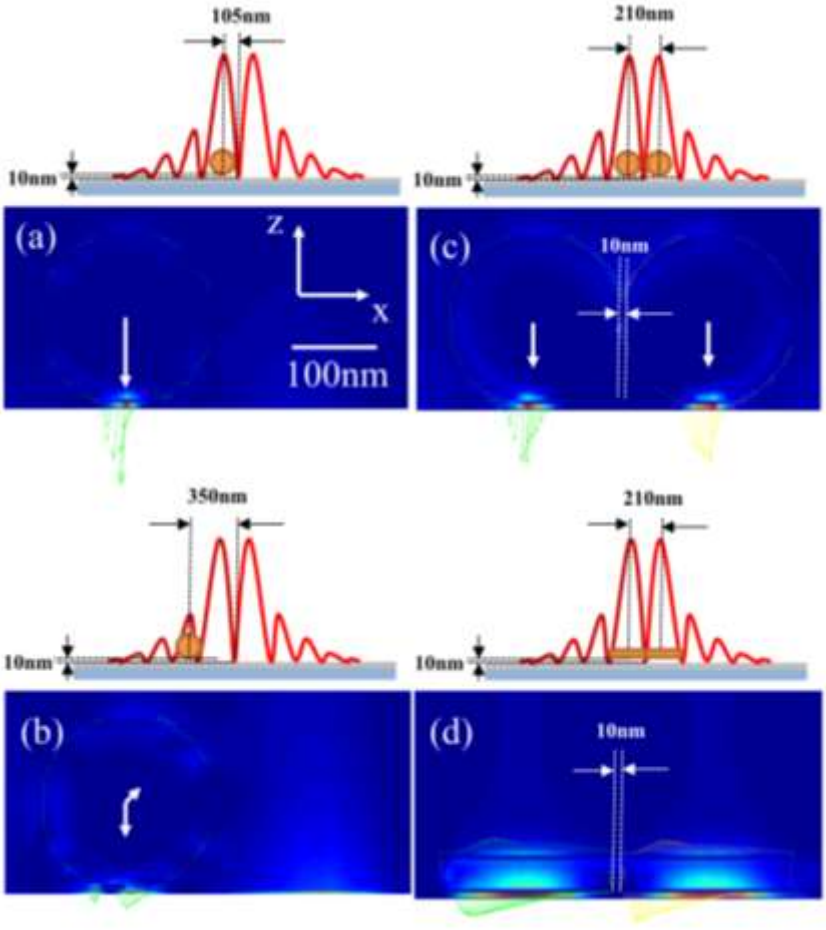

Fig. 2. The force analysis for: a single 200nm-diameter gold nanosphere (a) placed on the left virtual probe, 0.1μm off the center and (b) placed 0.35μm off the center; (c) Two gold nanospheres (diameter 200nm), trapped by the plasmonic field; and (d) two gold nanorods (200nm long and 40nm in diameter). Green and yellow arrows show the force around the particle in X-Z plane. The white arrows show the total force. The schematic diagrams show the locations of particles in the plasmonic field.

We further investigated the trapping of nanorods in our system, as the nanorod is a common type of nanoparticles and can be easily synthesized in solution. Fig. 2(d) showed the force distribution around the nanorods. The forces exerted on both nanorods were similar, leading to a stable spacing. The trapping force was resulted from the coupling between SPP and LSP. Essentially this was the interaction between charges. The free electrons were re-distributed by polarization as a result of interaction between the optical field and free electrons. Our results demonstrated that other nanoparticles at different shapes and sizes can be trapped by the plasmonic field in the system described here.

In order to explain the plasmonic trapping mechanisms, we calculated the exerted forces on a gold nanosphere at different locations in the plasmonic field. Firstly, the particle was placed above the left plasmonic lobe and was moved away from the substrate along z direction. It can be seen in Fig. 3(a) that the force increased exponentially when the particle was moved closer to the substrate. As was proven by Zhan et al. [37], since the excited field was a non-diffraction field, the force distributions in x direction remain similar for particles with different z coordinates. Fig. 3(b) showed how forces varied in x direction. The plasmonic-field force was strongest at around 100nm (the location of the virtual probe) to the

center and became smaller when moved away from the center. The fluctuation was a result of the Bessel distribution of the plasmonic field. In Fig. 3 (c), we calculated the forces in x direction. It can be seen that the force in x direction (F_x) was much smaller than the force in z direction (F_z), and therefore forces in z direction was dominant in particle trapping. In addition, as was shown in Fig. 3(c), when the distance to the center was less than 0.615μm, the force became an attracting force, which moved the particle towards the virtual probe.

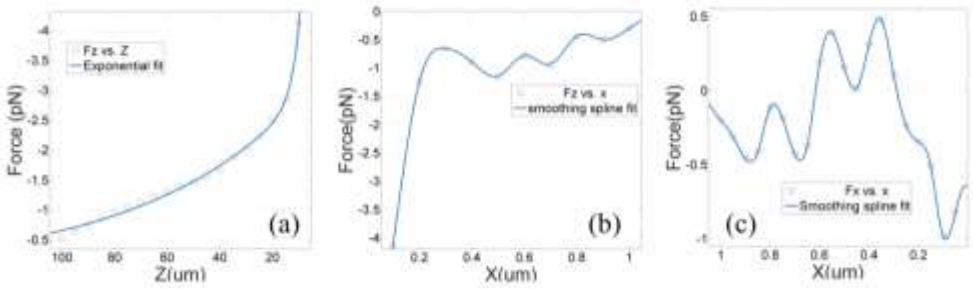

Fig. 3 Calculated forces on gold nanoparticles in the plasmonic field when: (a) the gold nanoparticle was placed above the trapping lobe and moved towards the Ag-film substrate (z =0). Negative force means the force direction is in negative z; (b) the gold nanoparticle was placed on the Ag film and moved away from the center of virtual probe (x = 100nm) in x direction; and (c) the calculated force in x direction under the same condition as that in (b), and the negative force means the direction away from the center.

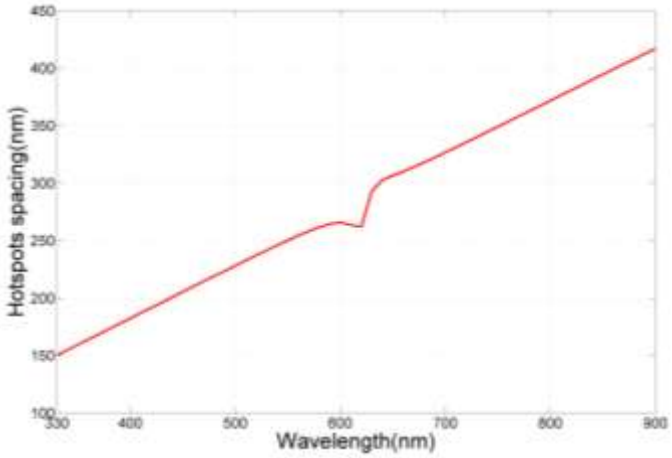

Fig. 4 Calculated virtual-probe-pair spacing as a function of the incident light wavelength

We also studied the possibility of controlling the spacing between the two virtual probes for dimer-spacing control. This spacing can be calculated by using Eq. (12). We assumed that the two virtual probes were located on x axis and the light was linearly-polarized in x direction ($\varphi = 0$). Since the transmission efficiency for p-polarization components was maximum at θ_{sp}, we can obtain the relation $E_t(\rho) \propto J_1(k_2 \rho \sin\theta_{sp})$ based on Eq. (12), by using θ_{sp} as the integration variable. Therefore, the virtual-probe spacing was a function of θ_{sp}, as $k_i = k_0 n_i$ can be regarded as a constant. According to Equations (1) and (2), θ_{sp} was determined by both the incident wavelength and the permittivity of Ag. The permittivity of Ag was wavelength-dependent and can be approximated based on Drude-Lorentz model described in [38]. Therefore, the virtual-probe was a function of the excitation wavelength and the calculated virtual-probe pair spacing as a function of the incident wavelength was given in Fig. 4. This suggested that the particle spacing in the dimer can be tuned by changing the excitation wavelengths.

Finally we investigated the LSPR and the field enhancement in our system. We used the relation $EF_{Raman} \approx \left|\frac{E_{loc}}{E_{in}}\right|^4$ to estimate the filed enhancement (where E_{in} is the incident electrical field, and E_{loc} denotes the local electrical field) [39]. In Fig. 5(a), the SPP was excited by a linearly-polarized beam. Two strong LSPRs can be seen clearly, leading to an enhancement of ~20 times, which agreed well with the theoretical results based on Fresnel transmission calculation [Fig. 1 (c)]. The field distribution in Z direction matched the force curve shown in Fig. 3(a). By placing a single gold nanosphere on the Ag film as was shown in Fig. 5(b), the SPR became more localized with a greater enhancement near 130 in the 10nm gap between the particle and the film, while the other virtual probe reduced in intensity due to the strong absorption resulted from the gold nanosphere. Fig. 5(c) showed that when a dimer was introduced into our system. The gap of the gold nanosphere dimer was set to 10nm and the distance between the nanospheres and the film remained at 10nm. The hot spots were localized in the gaps between the particles and the film, and no strong LSPR was observed between two nanoparticles. This was because that LSPR is dependent on the direction of polarization of the incident light. The plasmonic field in the dimer gap was perpendicular to the light polarization direction, which led to a weaker LSPR. In Fig. 5 (c), the field enhancements for both particle-film gaps were about 60 (less than half of 130). Strong LSPR in particle-film gaps and weak LSPR between particles was a result of the plasmonic field distribution. Further comparison was made in Fig. 5(d) to show the potential applications of trapped gold nanoparticle dimer in SERS. An excitation beam linearly-polarized in x direction was used to achieve a field enhancement factor near 1300.

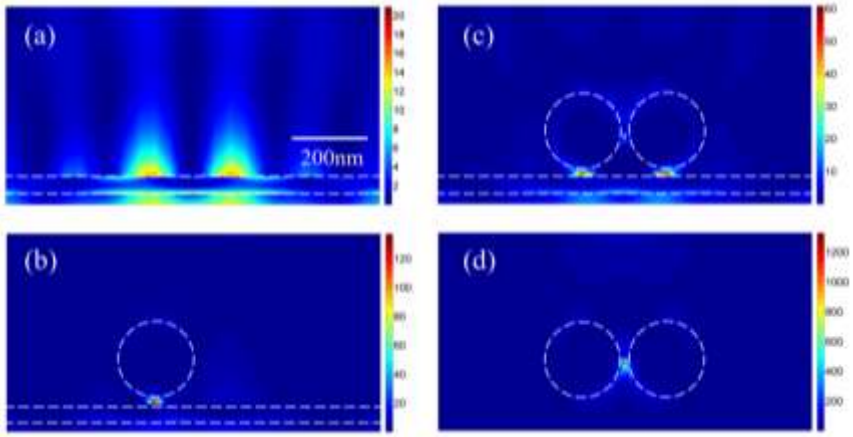

Fig. 5. The calculated field enhancement in x-z plane, when: (a) no gold particles, (b) one gold nanosphere placed on the Ag film, (c) a gold nanosphere dimer placed on the gold film. (d) the nanosphere dimer was illuminated by a focused linearly polarized beam, the polarization direction in horizontal. Dashed circles are the gold nanospheres (Diameter: 200nm). The gap between the Ag film and the nanoparticle is 10nm. The spacing between two nanospheres in the dimer is 10nm. The dashed lines are the top and bottom of the Ag film (Thickness: 45nm).

4. Conclusion

In conclusion, we presented a plasmonic trapping system for manipulating and tuning the metallic nanoparticle dimers. We found that two virtual probes in the plasmonic field with strong field concentration can be formed by focused linearly-polarized beam excitation. These virtual probes were capable of trapping multiple metallic particles. Our simulation showed that two free-standing nanoparticles, such as nanospheres or nanorods, can be trapped simultaneously in this proposed plasmonic trapping system. We also proved theoretically that

the gap spacing between the nanoparticles in the dimer can be tuned by changing the excitation wavelength. The work presented in this paper is believed to be the first study on multiple-nanoparticle trapping without using structured light. We consider this as a step towards the development of new plasmonic trapping technologies for multiple metallic particles, where no nanofabrication is involved. Our technique can be combined with other technologies or trapping methods and may achieve a high resolution beyond the diffraction limit for nanoscale manipulation. The proposed method may serve as a new way of realizing strong LSPR hot spots for SERS detections with single molecule sensitivity.

Acknowledgments

This work was supported by the Engineering and Physical Sciences Research Council [grant number EP/L022559/1]. Z.S. gratefully acknowledges the financial support from China Scholarship Council (No. 201408060330).